processes

MDPI

Article

Effect of the Preparation Method on the Physicochemical Properties and the CO Oxidation Performance of Nanostructured CeO_2/TiO_2 Oxides

Sofia Stefa [1], Maria Lykaki [1], Dimitrios Fragkoulis [1], Vasileios Binas [2], Pavlos K. Pandis [3], Vassilis N. Stathopoulos [3,*] and Michalis Konsolakis [1,*]

1 Industrial, Energy and Environmental Systems Lab (IEESL), School of Production Engineering and Management, Technical University of Crete, GR-73100 Chania, Greece; sstefa@isc.tuc.gr (S.S.); mlykaki@isc.tuc.gr (M.L.); dimifragkoulis@uoa.gr (D.F.)

2 Institute of Electronic Structure and Laser (IESL), FORTH, P.O. Box 1527, Vasilika Vouton, GR-71110 Heraklion, Greece; binasbill@iesl.forth.gr

3 Laboratory of Chemistry and Materials Technology, General (Core) Department, National and Kapodistrian University of Athens, GR-34400 Psachna Campus, Greece; ppandis@uoa.gr

* Correspondence: vasta@uoa.gr (V.N.S.); mkonsol@pem.tuc.gr (M.K.); Tel.: +30-22280-99688 (V.N.S.); +30-28210-37682 (M.K.)

Received: 24 June 2020; Accepted: 14 July 2020; Published: 16 July 2020

Abstract: Ceria-based mixed oxides have been widely studied in catalysis due to their unique surface and redox properties, with implications in numerous energy- and environmental-related applications. In this regard, the rational design of ceria-based composites by means of advanced synthetic routes has gained particular attention. In the present work, ceria–titania composites were synthesized by four different methods (precipitation, hydrothermal in one and two steps, Stöber) and their effect on the physicochemical characteristics and the CO oxidation performance was investigated. A thorough characterization study, including N_2 adsorption-desorption, X-ray diffraction (XRD), scanning electron microscopy with energy dispersive X-ray spectroscopy (SEM/EDS), transmission electron microscopy (TEM) and H_2 temperature-programmed reduction (H_2-TPR) was performed. Ceria–titania samples prepared by the Stöber method, exhibited the optimum CO oxidation performance, followed by samples prepared by the hydrothermal method in one step, whereas the precipitation method led to almost inactive oxides. CeO_2/TiO_2 samples synthesized by the Stöber method display a rod-like morphology of ceria nanoparticles with a uniform distribution of TiO_2, leading to enhanced reducibility and oxygen storage capacity (OSC). A linear relationship was disclosed among the catalytic performance of the samples prepared by different methods and the abundance of reducible oxygen species.

Keywords: CeO_2/TiO_2 mixed oxides; Stöber method; ceria nanorods; CO oxidation

1. Introduction

Ceria (CeO_2) has attracted significant attention in heterogeneous catalysis due to its enhanced properties such as high oxygen storage capacity (OSC) and thermal stability, [1–3]. The facile shift between two oxidation states (Ce^{3+}/Ce^{4+}), followed by the generation of surface/structural defects, e.g., oxygen vacancies, is responsible for its improved redox behaviour [1,4–7]. More importantly, the development of ceria particles in the nanoscale is of great significance as a decrease in the particle size can lead to distinct physicochemical properties as compared to their bulk counterparts, such as high specific surface area, tunable pore size, abundant defects and adjustable surface chemistry [8–11].

In addition, ceria-based metal oxides are extensively investigated in heterogeneous catalysis as supporting carriers or catalysts by themselves due to their surface and structural features which are totally different from those of parent oxides [2,3,12–23]. The synergetic interaction between the different counterparts usually leads to distinct physicochemical properties with a great impact on catalytic activity. Among the mixed oxides, transition metal-based oxide catalysts are of particular importance, due to their peculiar chemisorption properties. The incorporation of various transition metals into the ceria carrier can lead to significant physicochemical perturbations through the geometric and/or electronic interactions developed between the different counterparts [2,24–28].

In this regard, the addition of titanium oxide (TiO_2) in the lattice of ceria can significantly affect its physicochemical and redox properties and thus, its catalytic behaviour. Moreover, although TiO_2 is being widely used as a semiconductor photocatalyst, its wide band gap (3.0–3.2 eV) and the facile electron-hole pairs recombination limit its photocatalytic performance [26,29]. In this direction, its combination with ceria is considered quite promising due to ceria's narrow band gap and reversible redox couple (Ce^{3+}/Ce^{4+}) [29]. CeO_2/TiO_2 mixed oxides have been studied, among others, for the removal of volatile organic compounds (VOCs), the photocatalytic degradation of organic pollutants, the partial oxidation of methane, the steam reforming of ethanol, the oxidation of CO, etc. [29–39].

Different methods have been used for the preparation of ceria–titania mixed oxides, such as hydrothermal [29,36,37,40–44], co-precipitation [36,45–47], sol–gel [35,48,49], microemulsion [50], incipient wetness impregnation [51], etc. The preparation method greatly affects the morphology as well as the surface properties of CeO_2/TiO_2 composites leading to various nanostructures, such as core-shell spheres, nanoparticles or nanorods [40,44,52], flower-like heterostructures, nanorods and nanoparticles [36,42]. For instance, Li et al. [36] synthesized ceria–titania nanorods and nanoparticles through the hydrothermal and co-precipitation methods, respectively, in order to use them as the noble metal's supports, revealing a strong CO oxidation performance of the nanorod-like morphology of the CeO_2/TiO_2 support. Also, CeO_2/TiO_2 catalysts were prepared by three methods (impregnation, co-precipitation, and single-step sol-gel) with the sol–gel method resulting in the highest activity for the selective catalytic reduction of NO with NH_3, due to the high surface area of the composites, their good reducibility and the strong ceria–titania interaction [53].

The oxidation of CO has been extensively used as probe reaction in various catalytic systems in order to fully comprehend the structure–property relationships [54–57]. The employment of such a reaction in the present study could give precious information and feedback regarding the catalytic behaviour of ceria–titania composites towards their application as catalysts or supporting carriers in diverse energy- and environmental-related applications.

In view of the above aspects, the objective of the present work is to explore the impact of synthesis procedure, i.e., one- and two-stage hydrothermal method, precipitation, Stöber [58,59] on the physicochemical characteristics and the CO oxidation performance of CeO_2/TiO_2 mixed oxides. The as-prepared materials were thoroughly characterized by N_2 physisorption, XRD, SEM/EDS, TEM, and H_2-TPR, while their catalytic behaviour was evaluated in the CO oxidation reaction to reveal structure–property relationships.

2. Materials and Methods

2.1. Materials Synthesis

The chemical compounds used in this work were of analytical grade. $TiOSO_4$ (purity ≥ 29%, Sigma-Aldrich, St. Louis, MO, USA) $Ce(NO_3)_3{\cdot}6H_2O$ (≥99.0%, Fluka, Bucharest, Romania) and tetrabutyl titanate (TBOT, purity ≥ 97%, Sigma-Aldrich, St. Louis, MO, USA) were employed as precursors for the synthesis of ceria–titania samples. NH_3 (25 vol.%, Sigma-Aldrich, St. Louis, MO, USA), NaOH (≥98%, Honeywell Fluka, Seelze, Germany) and absolute EtOH (≥99.8%, ACROS Organics, Geel, Belgium) were also used during preparation.

CeO_2/TiO_2 mixed oxides with Ce/Ti atomic ratio of 4 were prepared by various methods, namely, precipitation, hydrothermal in one and two steps, and Stöber. This specific ratio was dictated from our previous studies on ceria-based mixed oxides [18–20].

Ceria–titania by precipitation (CeO_2/TiO_2-P) was prepared as follows: initially, 10.4 mmol $Ce(NO_3)_3{\cdot}6H_2O$ and 2.6 mmol $TiOSO_4$ were dissolved in double deionized water (0.50 M) in order to achieve complete dissolution of the precursors. Then, NH_3 (25 vol.%) was added at room temperature (RT) to the solution under constant stirring until pH reached the value of 10. After 3 h of stirring the resulting formulation was centrifuged and washed with double deionized water and EtOH. The precipitate was treated at 90 °C for 12 h and 500 °C for 2 h under air flow (heating rate 5 °C min^{-1}) [33].

Ceria–titania by one-step hydrothermal (CeO_2/TiO_2-H1) was prepared as follows: initially, 3.0 mol NaOH was added in 75 mL of water. An aqueous solution of 175 mL containing 20 mmol of $Ce(NO_3)_3{\cdot}6H_2O$ and 5.0 mmol of $TiOSO_4$ (0.14 M) was then added under vigorous stirring in the above solution until a milky slurry was formed. The mixture was left for 1 h of additional stirring and the final slurry was placed in a Teflon vial and aged for 24 h at 90 °C. The materials were thoroughly washed with double deionized water until pH 7, followed by EtOH washing as to avoid nanoparticles agglomeration. Finally, the precipitate was dried for 12 h at 90 °C and calcined at 500 °C for 2 h under air (heating rate 5 °C min^{-1}) [36].

Ceria-titania by two-step hydrothermal synthesis (CeO_2/TiO_2-H2) was prepared as follows: bare ceria nanorods (CeO_2 NRs) were initially prepared by the hydrothermal method, as mentioned above in the one-step hydrothermal method, with the variation of utilizing 25 mmol $Ce(NO_3)_3{\cdot}6H_2O$ instead of 20 mmol and the absence of $TiOSO_4$. Then, CeO_2/TiO_2 nanorods were prepared by a wet-chemical method. Typically, 0.15 g of bare ceria nanorods was dispersed into 200 mL of double deionized water under vigorous stirring and 0.035 g $TiOSO_4$ was dissolved into 1.1 mL of double deionized water and added into the aforementioned suspension at room temperature. The mixture was left for additional stirring for 3 h and aged at room temperature for 2–3 h. The precipitate was dried for 12 h at 90 °C, followed by calcination at 500 °C for 2 h under air (heating rate 5 °C min^{-1}) [40].

Ceria–titania by Stöber method (CeO_2/TiO_2-S) was prepared as follows: bare ceria nanorods were initially synthesized by the hydrothermal method as previously described. 0.25 g of bare ceria nanorods were dispersed in 334 mL of absolute ethanol and mixed with 1 mL concentrated ammonia solution (28 wt.%) under ultrasonication for 20 min. Then, 0.125 mL TBOT was added dropwise and the solution was left stirring at 45 °C for 24 h. The resulting precipitate was recovered by centrifugation and washed with double deionized water and ethanol. The precipitate was dried for 12 h at 90 °C, followed by calcination at 500 °C for 2 h under air (heating rate 5 °C min^{-1}) [29].

2.2. Materials Characterization

The textural features of the as-prepared samples were evaluated by N_2 adsorption–desorption using a Nova 2200e Quantachrome flow apparatus (Quantachrome Instruments, Florida, USA). Surface area (m^2 g^{-1}) was calculated using the Brunauer–Emmett–Teller (BET) method applied in the 0.05–0.30 range of relative pressures [60,61]. At the highest relative pressure, the specific pore volume (cm^3 g^{-1}) was obtained. The Barrett–Joyner–Halenda (BJH) method was applied to determine the average pore size diameter (dp, nm). Prior to measurement all samples were outgassed at 250 °C for 5 h under vacuum.

Crystallinity of the samples was investigated by powder X-ray diffraction (XRD) in a Rigaku diffractometer (model RINT 2000) (Rigaku, Tokyo, Japan) using Cu Kα radiation (λ_{Ka} = 0.154 nm, 40 kV/80 mA) in the range of 10° to 80° with a step of 0.05° min^{-1}. The primary crystallite size of the samples was calculated by applying the Scherrer Equation (1):

$$D_{XRD}\ (\mathrm{nm}) = \frac{K\lambda}{\beta \cos\theta} \quad (1)$$

where λ: wavelength of the X-ray in nm, K: Scherrer constant, B: line broadening, θ: Bragg angle. By using the Scherrer Equation (1), on the most intense diffraction peak, i.e., for CeO_2 (2θ: 28.5°), the primary particle size of this crystal phase was determined.

Morphological characterization of the samples was determined by scanning electron microscopy (SEM, JSM-6390LV, JEOL Ltd., Tokyo, Japan) working at 20 keV, coupled with an energy dispersive X-ray spectrometry (EDS) system. The samples in the form of powders were sputtered with Au to create a coating with a thickness of 10 nm, approximately. Furthermore, the samples were imaged by transmission electron microscopy (TEM) using a JEM-2100 instrument (JEOL, Tokyo, Japan) equipped with LaB_6 filament, working at 200 kV. TEM specimens were prepared by deposition of dispersed powder samples by ultrasonication.

The redox properties of as-prepared samples were assessed by temperature-programmed reduction with hydrogen as reducing agent (H_2-TPR). In a typical experiment, 100 mg of the sample was placed in a quartz fixed-bed reactor heated up to 800 °C with a rate of 20 K min^{-1}. Before TPR experiments, samples were treated up to 500 °C for 30 min under 20 vol.% O_2 in He (20 cm^3 min^{-1} flow), then cooled to 200 °C under the same gas mixture and finally to room temperature under pure He flow. A known quantity of CuO standard sample was used to quantify the H_2 uptake from the samples [62,63]. H_2 uptake (mmol H_2 g^{-1}), corresponding to the H_2 consumed by reducible oxygen species, is calculated by the integration of TPR peaks area. Oxygen Storage Capacity (OSC), in μmol O_2 g^{-1}, is determined as a half of this quantity [64].

2.3. Catalytic Activity Studies

Catalytic measurements were carried out in a quartz fixed-bed tubular microreactor (i.d.: 12.95 mm) under ambient pressure, loaded with 0.10 g of catalyst.

The reaction gas mixture consisted of 0.2 vol.% of CO and 1 vol.% O_2 both balanced with He. A total feed stream of 80 cm^3 min^{-1} was used, corresponding to a gas hourly space velocity (GHSV) of 40,000 h^{-1}.

Before catalytic tests, all samples were pretreated under 20 vol.% O_2 in He with a 20 cm^3 min^{-1} flow and heated to 480 °C for 30 min with a rate of 10 K min^{-1}. Consequently, samples were cooled to 25 °C at the same rate and purged with He in order to remove any physisorbed species. Catalytic performance evaluation was carried out up to 500 °C for each sample. CO and CO_2 were monitored by a Gas Chromatograph with two channels with independent thermal conductivity detectors, injectors and capillary columns, i.e., Molecular Sieve 5X, PoraPlot Q.

The CO conversion (X_{CO}) was calculated from the difference in CO concentration among inlet and outlet gas streams:

$$X_{CO}(\%) = \frac{[CO]_{in} - [CO]_{out}}{[CO]_{in}} \times 100 \quad (2)$$

where $[CO]_{in}$ and $[CO]_{out}$ are the CO concentration in the inlet and outlet gas streams, respectively.

Specific reaction rates of CO conversion (in mol g^{-1} s^{-1} or mol m^{-2} s^{-1}) were estimated under differential reaction conditions (X_{CO} < 15%, T = 200 °C, W/F = 0.075 g s cm^{-3}).

$$r\left(\frac{mol}{g{\cdot}s}\right) = \frac{X_{CO} \times [CO]_{in} \times F\left(\frac{cm^3}{min}\right)}{100 \times 60\left(\frac{s}{min}\right) \times V_m\left(\frac{cm^3}{mol}\right) \times m_{cat}(g)} \quad (3)$$

$$r\left(\frac{mol}{m^2{\cdot}s}\right) = \frac{X_{CO} \times [CO]_{in} \times F\left(\frac{cm^3}{min}\right)}{100 \times 60\left(\frac{s}{min}\right) \times V_m\left(\frac{cm^3}{mol}\right) \times m_{cat}(g) \times S_{BET}\left(\frac{m^2}{g}\right)} \quad (4)$$

F: total flow rate, V_m: gas molar volume; all at standard ambient temperature and pressure conditions (298 K, 1 bar), m_{cat}: catalyst's mass, S_{BET}: specific surface area.

3. Results and Discussion

3.1. Textural/Structural Characterization

In Table 1, the main textural and structural properties of bare CeO_2 and CeO_2/TiO_2 samples are presented. Ceria–titania prepared by the one-step hydrothermal method (CeO_2/TiO_2-H1) demonstrates the highest value in BET surface area (100.9 $m^2\ g^{-1}$), followed by bare CeO_2 NRs (73.9 $m^2\ g^{-1}$), CeO_2/TiO_2-S (72.0 $m^2\ g^{-1}$), CeO_2/TiO_2-H2 (63.2 $m^2\ g^{-1}$) and CeO_2/TiO_2-P (41.5 $m^2\ g^{-1}$). An increase in the surface area is observed for the CeO_2/TiO_2-H1 sample, as compared to bare CeO_2 NRs. In contrast, the BET surface area is decreased in the CeO_2/TiO_2-S, CeO_2/TiO_2-H2 and CeO_2/TiO_2-P samples. Apparently, the preparation procedure notably affects the textural/structural characteristics and in turn the surface area, as further discussed below.

Table 1. Textural/structural, redox properties of CeO_2 and CeO_2/TiO_2 samples.

Sample	BET Analysis			XRD Analysis	H_2-TPR	
	BET Area ($m^2\ g^{-1}$)	Pore Volume ($cm^3\ g^{-1}$)	Pore Size (nm)	Crystallite Size, D_{XRD} (nm) CeO_2	Oxygen Storage Capacity (mmol $O_2\ g^{-1}$)	Temperature of Peak Maximum (°C)
CeO_2 NRs	73.9	0.48	24.2	13	0.29	545
CeO_2/TiO_2-P	41.5	0.13	9.3	12	-	-
CeO_2/TiO_2-H1	100.9	0.41	15.0	9	0.34	654
CeO_2/TiO_2-H2	63.2	0.48	24.1	14	-	-
CeO_2/TiO_2-S	72.0	0.58	32.0	12	0.79	573

The BJH pore size distribution (PSD) of as-prepared samples is displayed in Figure 1a and the respective adsorption-desorption isotherms are shown in Figure 1b. In all samples, the pore size maxima are over 3 nm, signifying the existence of mesopores that can be further verified by the presence of type IV adsorption–desorption isotherms (Figure 1b). The CeO_2/TiO_2-S sample exhibits the highest pore size (32.0 nm), followed by CeO_2 NRs (24.2 nm), CeO_2/TiO_2-H2 (24.1 nm), CeO_2/TiO_2-H1 (15.0 nm) and CeO_2/TiO_2-P (9.3 nm) and it also shows a broader PSD than the rest samples.

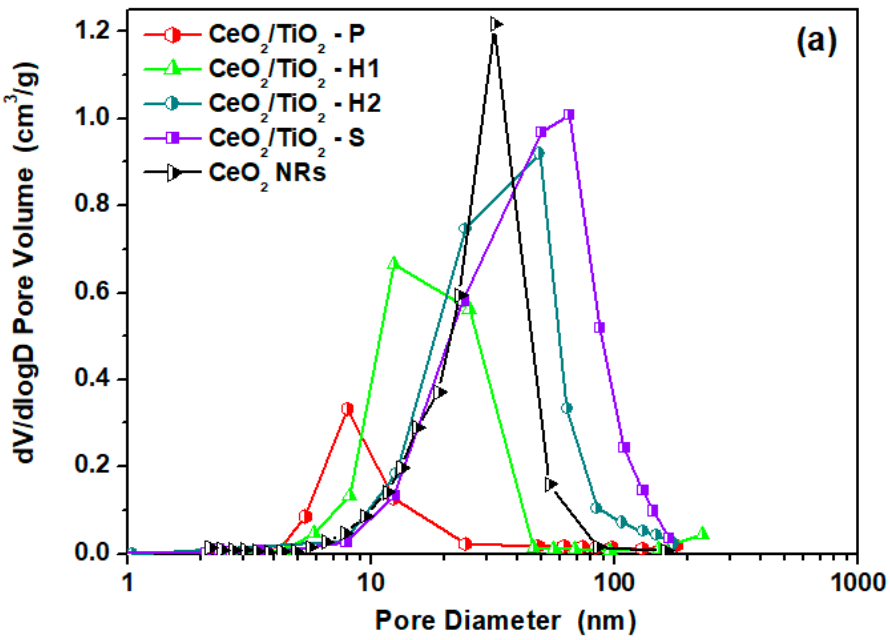

Figure 1. *Cont.*

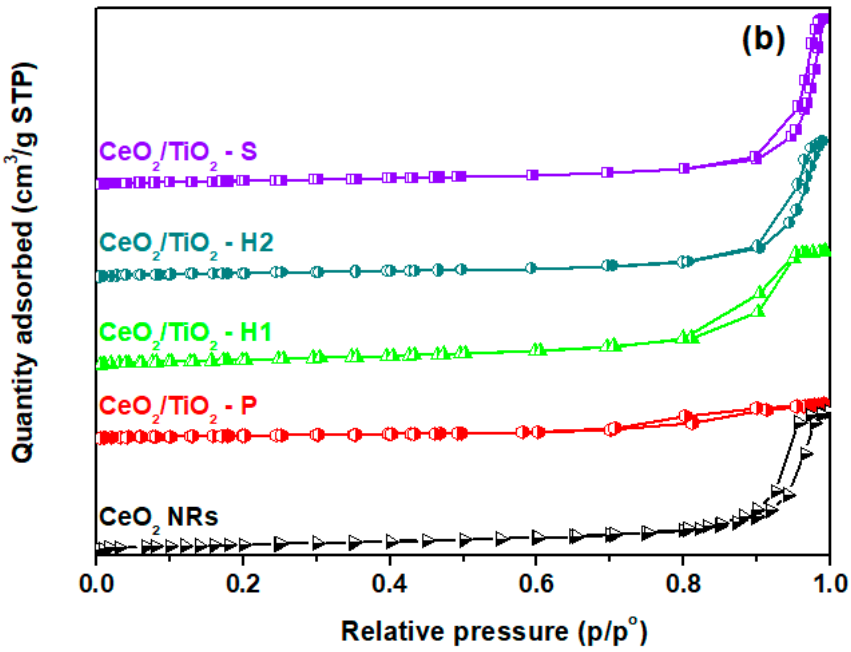

Figure 1. (**a**) BJH desorption pore size distribution; (**b**) adsorption-desorption isotherms of bare CeO_2 and CeO_2/TiO_2 samples.

Figure 2 exhibits the XRD patterns of all samples. The main diffraction peaks which correspond to the following planes: (111), (200), (220), (311), (222), (400), (331) and (420) are ascribed to the face-centered cubic fluorite structure of ceria (Fm3m symmetry, no. 225) [65–67]. The titanium oxide phase is hardly detected only in the CeO_2/TiO_2-S sample, with a small peak at 2θ value ~25°, which corresponds to the anatase (TiO_2) phase [68–71]. The difficulty in detecting the TiO_2 phase in the XRD patterns is probably related to the low TiO_2 loading in combination with its high dispersion. By applying the Scherrer Equation (1), the primary crystallite size of ceria was calculated (Table 1) within the approximation degree induced by the method. Bare ceria shows a crystallite size of 13 nm, with the CeO_2/TiO_2-H1, CeO_2/TiO_2-S, CeO_2/TiO_2-P and CeO_2/TiO_2-H2 samples exhibiting crystallite sizes of 9, 12, 12 and 14 nm, respectively. Apart from the sample prepared by the two-step hydrothermal method (CeO_2/TiO_2-H2), all the other ceria–titania samples exhibit a small reduction in the crystallite size of ceria. The small differences in ceria crystallite size and morphology upon the introduction of different synthetic protocols could be ascribed to the impact of various parameters (extent of calcination, interaction between heteroatoms, etc.) on the growth rate of ceria nanoparticles [72–74].

3.2. Morphological Characterization (TEM, SEM-EDS)

The morphological characteristics of the ceria–titania nanostructures were investigated by transmission electron microscopy analysis. In Figure 3, the TEM images of bare ceria nanorods and of CeO_2/TiO_2 mixed oxides are depicted. A bare ceria sample (Figure 3a) displays a rod-like morphology with 50–200 nm in length. CeO_2/TiO_2-P (Figure 3b) exhibits irregular shapes, while CeO_2/TiO_2 mixed oxides synthesized by the hydrothermal method (one or two steps) also show the rod-like morphology (Figure 3c–f). In particular, the CeO_2/TiO_2-H1 sample exhibits smaller-sized nanorods (25–100 nm), as compared to bare CeO_2 NRs, while no separated TiO_2 particles are detected. Although the CeO_2/TiO_2-H2 sample also exhibits the rod-like morphology, distinct TiO_2 nanoparticles in contact with nanorods are clearly observed (Figure 3f). In Figure 3g, the CeO_2/TiO_2-S sample is depicted, showing a rod-like morphology (50–200 nm) without any separated TiO_2 particles being observed. The HRTEM (high-resolution transmission electron microscopy) results of CeO_2/TiO_2-S sample are displayed in Figure 3h. The lattice spacing of 0.36 nm is ascribed to the TiO_2 (101) crystal plane, and the lattice spacings of 0.31 and 0.19 nm are ascribed to the CeO_2 (111) and (220) crystal

planes, respectively [5,8,17,29,32,33,75,76]. Therefore, it can be argued that, in the case of CeO_2/TiO_2-S sample, a uniform distribution of TiO_2 around ceria nanorods can be obtained.

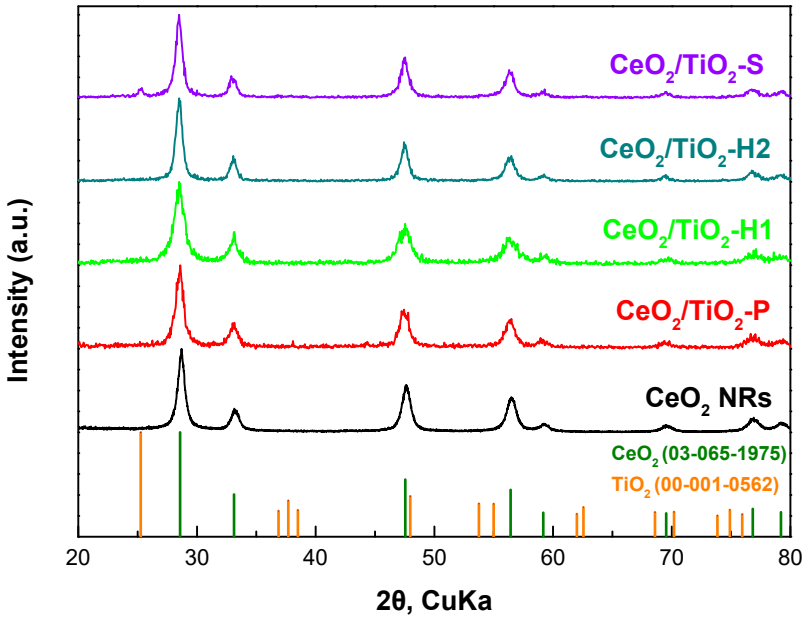

Figure 2. XRD patterns of CeO_2 and CeO_2/TiO_2 samples.

In addition, the elemental mapping of CeO_2/TiO_2 samples was carried out by SEM/EDS analysis (Figure 4). The SEM images of ceria–titania mixed oxides are illustrated below (Figure 4a,e,i,m), along with the corresponding elemental mapping images (Figure 4b–d,f–h,j–l,n–p). A uniform distribution of Ce, Ti, O elements in the ceria–titania mixed oxides can be observed from SEM/EDS analysis.

3.3. Redox Properties (H_2-TPR)

For reactions proceeding via a surface reduction step such as CO oxidation, H_2-TPR results can identify and quantify the active oxygen sites of the catalysts. Figure 5 depicts the reduction profiles of as-prepared samples in the temperature range of 100–800 °C. The samples CeO_2/TiO_2-S, CeO_2/TiO_2-H1 and CeO_2-NRs show a peak in the low temperature region of 500–700 °C, which can be attributed to the relatively weakly bound surface oxygen species, in contrast to bulk oxygen, which is reduced at temperatures higher than ca. 750 °C. Interestingly, the CeO_2/TiO_2-P and CeO_2/TiO_2-H2 samples do not exhibit any reduction peaks in the temperature region investigated, revealing their inferior reducibility. The latter is in complete agreement with their negligible catalytic performance, as discussed later. Moreover, it is worth noticing that TiO_2 addition to CeO_2 leads to a shift of TPR peaks to higher temperatures (Table 1) as compared to bare CeO_2 NRs, implying the inhibition induced by TiO_2 incorporation on the detachment of surface oxygen species during the reduction process. On the other hand, significant differences were obtained in relation to H_2 uptake, corresponding to main TPR peaks (Table 1). CeO_2/TiO_2-S exhibited the highest value (1.58 mmol H_2 g^{-1}) followed by CeO_2/TiO_2-H1 (0.68 mmol H_2 g^{-1}) and CeO_2-NRs (0.58 mmol H_2 g^{-1}), resulting in OSC values of 0.79, 0.34 and 0.29 mmol O_2 g^{-1}, respectively. This finding clearly reveals that the TiO_2 incorporation into CeO_2 via the Stöber method, leads to an almost 3-fold increase in the population of reducible/active oxygen species, which are expected to determine the oxygen exchange kinetics and in turn, the CO oxidation process via a Mars-van Krevelen mechanism. In this point, it should be mentioned that the differences in the reducibility could be mainly attributed to the different extent of ceria–titania interactions, revealing the significance of the preparation method on the intrinsic characteristics of mixed oxides. In view of this fact, a close relationship was disclosed between the catalytic activity and OSC (see below), corroborating the above arguments.

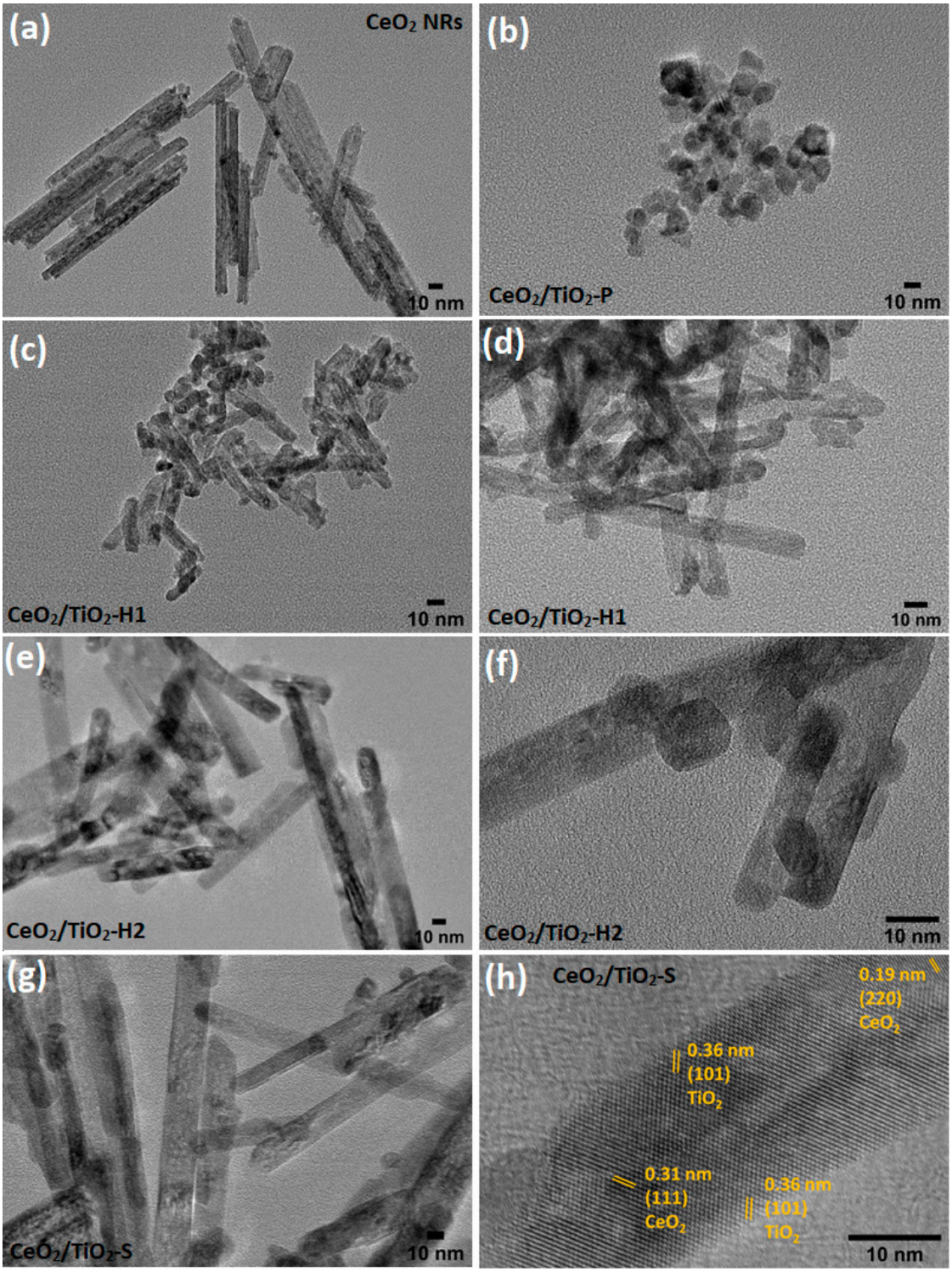

Figure 3. TEM images of the samples: (**a**) CeO_2-NRs; (**b**) CeO_2/TiO_2-P; (**c**,**d**) CeO_2/TiO_2-H1; (**e**,**f**) CeO_2/TiO_2-H2; (**g**) CeO_2/TiO_2-S; (**h**) HRTEM images of CeO_2/TiO_2-S.

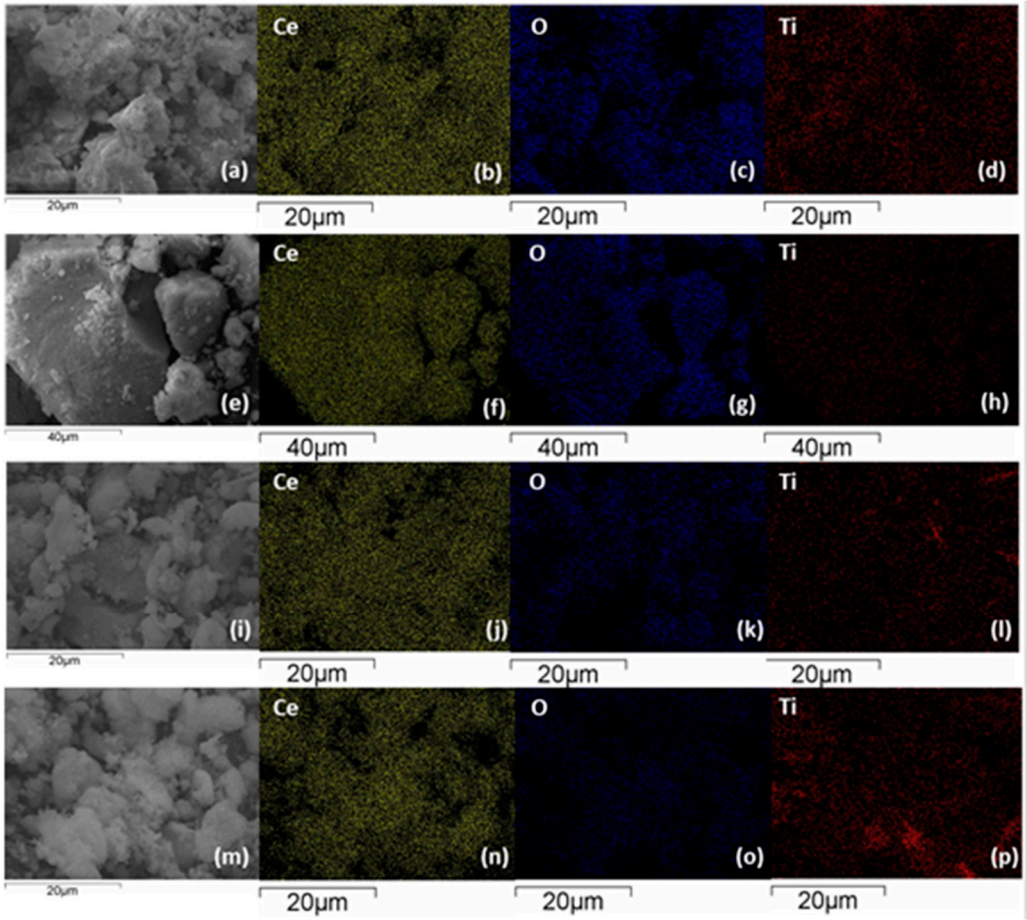

Figure 4. SEM and elemental mapping images of the samples: (**a**–**d**) CeO_2/TiO_2-P; (**e**–**h**) CeO_2/TiO_2-H1; (**i**–**l**) CeO_2/TiO_2-H2; (**m**–**p**) CeO_2/TiO_2-S.

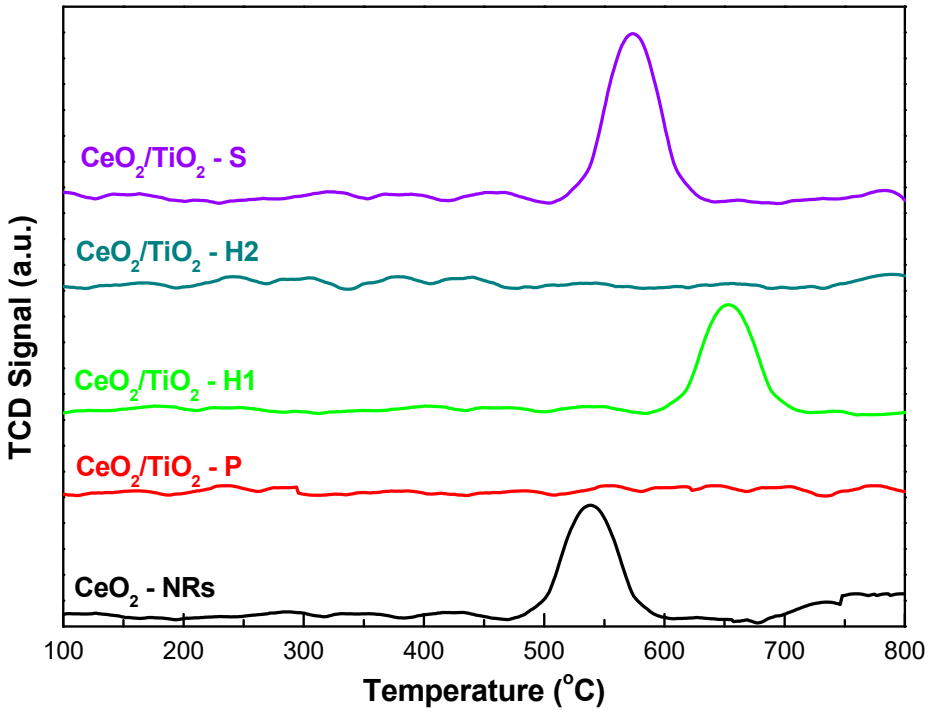

Figure 5. H_2-TPR profiles of CeO_2-NRs and CeO_2/TiO_2 samples.

3.4. Catalytic Evaluation Studies

To gain insight into the impact of the different preparation methods on the catalytic performance of the CeO_2/TiO_2 samples, their CO oxidation performance was investigated. Figure 6 depicts the conversion of CO with temperature for CeO_2 and CeO_2/TiO_2 samples. For comparison purposes, a TiO_2 commercial sample (Evonik industries) was also employed as reference material. A strong dependence between the preparation method and the nanostructure is observed, in accordance to our previous results [19]. As it becomes obvious from Figure 6, the sample prepared by the Stöber method (CeO_2/TiO_2-S) exhibits the best CO conversion performance among all samples tested. The bare ceria nanorods (CeO_2-NRs) and ceria–titania prepared by the one-step hydrothermal method (CeO_2/TiO_2-H1) exhibit similar catalytic behaviour but, in both cases, their profiles are shifted by approximately 30 degrees to higher temperature than CeO_2/TiO_2-S. Notably, ceria–titania mixed oxides prepared by the precipitation and two-step hydrothermal methods demonstrate negligible CO conversion performance, namely ~8% and 22% at 500 °C, respectively, implying the key role of synthesis procedure. Similarly, bare TiO_2 is practically inactive in the temperature range investigated.

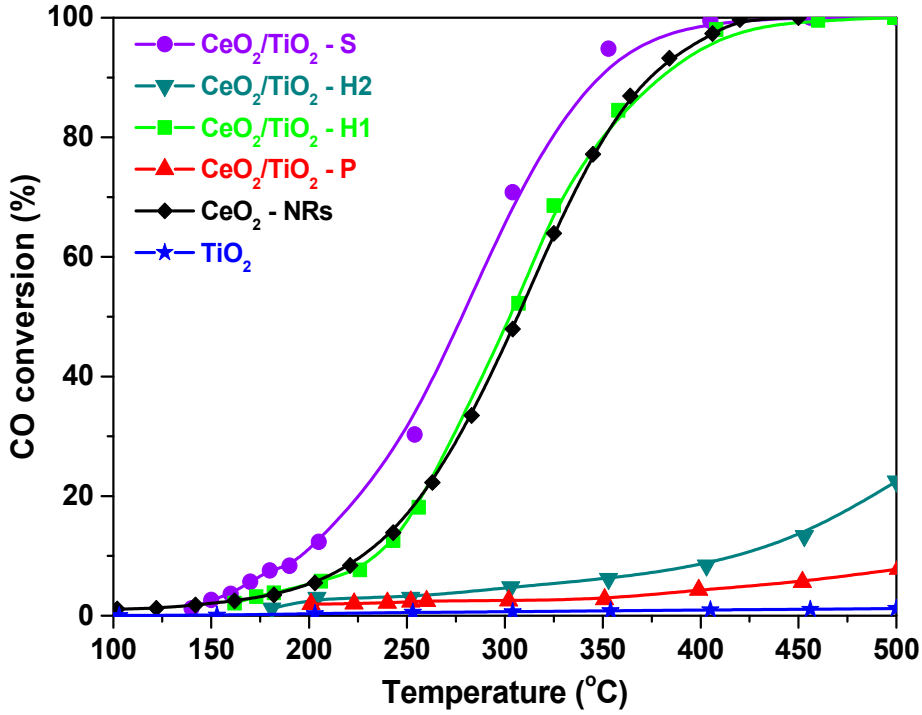

Figure 6. Conversion of CO with temperature for CeO_2, TiO_2 and CeO_2/TiO_2 samples. Reaction conditions: 0.2 vol.% CO, 1 vol.% O_2, GHSV = 40,000 h^{-1}.

In order to completely comprehend the impact of preparation procedure and catalyst composition (bare or mixed oxides) on the intrinsic reactivity, the different textural properties among the as-prepared samples (Table 2) should be taken into account. Hence, the specific activity, in terms of catalyst surface area (μmol m^{-2} s^{-1}) and mass (μmol g^{-1} s^{-1}) was calculated (Differential reaction conditions: X_{CO} < 15%, T = 200 °C, GHSV = 40,000 h^{-1}). Thus the relationship between CO oxidation activity and textural properties can be elucidated. Table 2 summarizes these results. Obviously, CeO_2/TiO_2-S demonstrates by far the optimum catalytic performance, in terms of conversion as well as of specific activity, further revealing its superiority. It should be also noted that a stable conversion performance (ca. 99% CO conversion) was attained at 400 °C in short-term (12 h) stability experiments.

Table 2. Conversion of CO and specific rates of CeO_2 and CeO_2/TiO_2 samples at 200 °C. Reaction conditions: 0.2 vol.% CO and 1 vol.% O_2 in He.

Sample	CO Conversion (%)	Specific Rate	
		r (μmol g^{-1} s^{-1})	r (×100) (μmol m^{-2} s^{-1})
CeO_2-NRs	5.1	0.056	0.075
CeO_2/TiO_2-P	1.9	0.021	0.050
CeO_2/TiO_2-H1	5.3	0.058	0.057
CeO_2/TiO_2-H2	3.0	0.033	0.052
CeO_2/TiO_2-S	11.1	0.121	0.168

The findings of the present work can be interpreted on the basis of a Mars-van Krevelen, redox-type mechanism, which mainly involves CO chemisorption towards the formation of $Ce^{\delta+}$-CO species, O_2 activation on the oxygen vacancies of ceria and active oxygen species formation [77,78]. The reaction is taking place among the chemisorbed CO and adjacent active oxygen, followed by the active sites regeneration and the replenishment of oxygen vacancies via gas phase oxygen participated in sequential catalytic cycles [77,78].

The pivotal role played by the redox properties during the CO oxidation process over CeO_2-based oxides is clearly described by the above mechanism. In particular, the high oxygen storage capacity of CeO_2/TiO_2-S sample (Table 1), linked to improved oxygen exchange kinetics and reducibility, can be considered responsible for its superior oxidation performance, as compared to the rest of the samples. In view of this fact, we recently showed, by means of both in situ and ex situ techniques, that the improved redox properties of CeO_2 composites of rod-like morphology, which are related to their abundance in defects and oxygen vacancies, is the decisive factor for their improved catalytic performance [18]. The above arguments concerning structure–activity relationships are clearly supported by the linear relationship among the specific reaction rate (μmol g^{-1} s^{-1}) and the redox properties (OSC, mmol g^{-1}), Figure 7.

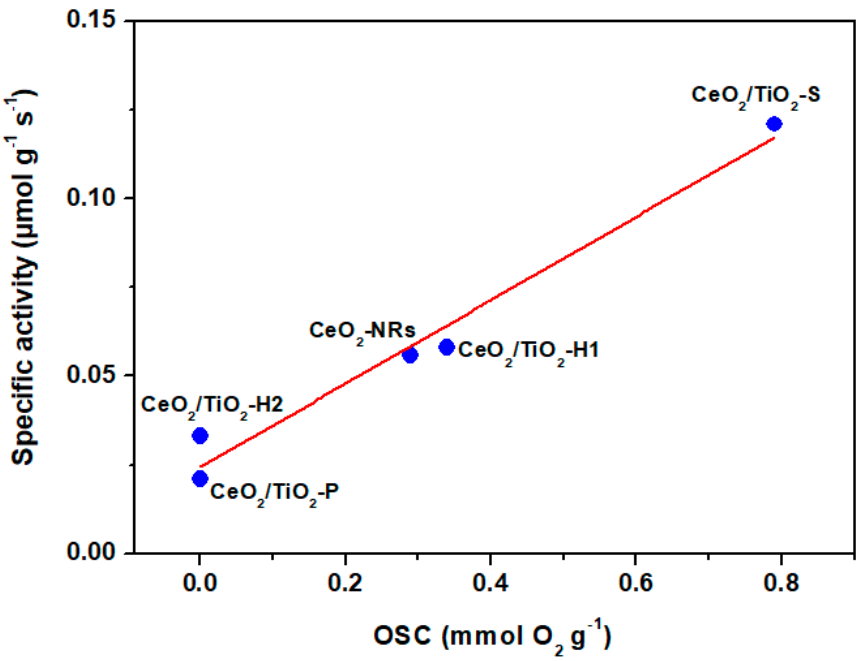

Figure 7. Relationship of the specific activity and the oxygen storage capacity of as-prepared samples.

In light of the above issues, the superiority of CeO_2/TiO_2-S catalyst can be ascribed to its higher population of weakly bound oxygen species, leading to enhanced oxygen storage capacity and reducibility, as identified by H_2-TPR. This can be attributed to the beneficial effect of Stöber method

towards obtaining highly homogenized composites of rod-like morphology, with no obvious separation between ceria and titania phases. In view of this fact, it can be argued that Stöber method could result to a synergistic ceria–titania interaction, which facilitates the formation of oxygen vacancies and the redox interplay between the interfacial sites, leading in turn to a higher population of active oxygen species. In good agreement to this, it has been revealed by means of DFT calculations that the formation of oxygen vacancies and Ce^{3+} sites is energetically favoured at the interface of ceria–titania [79].

Although bare titania is catalytically inert in CO oxidation, in contrast to CeO_2-NRs (Figure 6), their combination could lead to a synergistic interaction offering highly active CeO_2/TiO_2 mixed oxides. The latter, however, strongly depends on the synthesis procedure followed; the hydrothermal method in one or two steps does not alter (CeO_2/TiO_2-H1) or even worsen (CeO_2/TiO_2-H2) the catalytic activity as compared to bare ceria, in opposition to Stöber method. In particular, the introduction of titania into ceria nanorods by the hydrothermal method (CeO_2/TiO_2-H1) is clearly enhancing the textural properties (surface area), without however having an analogous effect on the catalytic performance. This can be explained by taking into account the distinctive shift of the TPR peak to higher temperature (Figure 5, Table 1), indicating a harder partial $Ce^{4+} \rightarrow Ce^{3+}$ reduction and detachment of O atoms, i.e., lower reducibility and an increase in oxygen vacancy formation energy. Moreover, no significant modifications were induced by the hydrothermal method on the concentration of reducible oxygen species, as verified by the similar OSC values between CeO_2-NRs and CeO_2/TiO_2-H1 samples (Table 1). On the other hand, although the Stöber method slightly inhibits surface oxygen reduction (shift of TPR peak to higher temperature), it drastically increases the population of active oxygen species, offering a ca. 3-fold increase in OSC compared to that provided by the hydrothermal method. Summarizing, the catalytic performance of CeO_2/TiO_2-S samples is superior to that of bare CeO_2, demonstrating the beneficial effect of a second oxide phase in conjunction to the synthesis procedure applied. These materials could be further employed as supporting carriers of various transition metals, boosting the transition to a noble metal free catalysis [3].

4. Conclusions

Ceria–titania mixed oxides were prepared by the hydrothermal, Stöber and precipitation methods. The CO oxidation was used as probe reaction to reveal possible structure–property relationships. The following order, in terms of CO conversion, was obtained: CeO_2/TiO_2-S > CeO_2/TiO_2-H1 > CeO_2-NRs > CeO_2/TiO_2-H2 > CeO_2/TiO_2-P > TiO_2. A characterization study by various complementary techniques revealed the significant effect of the synthesis procedure on the textural, morphological and redox features. Despite the inferior textural properties of the mixed oxides synthesized by the Stöber method, they exhibit the best catalytic performance, which can be ascribed to their improved reducibility, associated with their relative abundance in loosely bound oxygen species and high oxygen storage capacity. The Stöber method leads to rod-shaped ceria nanoparticles uniformly decorated by titania, which can be considered responsible for synergistic ceria–titania interactions towards an increased population of highly reducible active sites. The findings of the present study reveal that the rational design of mixed metal oxides without noble metals in their composition could provide the base for a wide range of materials, which could be used as catalysts or supporting carriers in various environmental and energy applications.

Author Contributions: S.S., M.L., D.F., V.B. and P.K.P. contributed to materials synthesis and characterization, results interpretation and paper-writing; V.N.S. and M.K. contributed to the conception, design, results interpretation and writing of the paper. All authors have read and agreed to the published version of the manuscript.

Funding: This research has been co-financed by the European Union and Greek national funds through the Operational Program Competitiveness, Entrepreneurship and Innovation, under the calls RESEARCH—CREATE—INNOVATE (project code: T1EDK-00094) and ERA-NETS 2018 (project code: T8EPA2-00005).

Conflicts of Interest: The authors declare no conflict of interest.

References

1. Montini, T.; Melchionna, M.; Monai, M.; Fornasiero, P. Fundamentals and Catalytic Applications of CeO_2-Based Materials. *Chem. Rev.* **2016**, *116*, 5987–6041. [CrossRef] [PubMed]
2. Konsolakis, M. The role of Copper–Ceria interactions in catalysis science: Recent theoretical and experimental advances. *Appl. Catal. B Environ.* **2016**, *198*, 49–66. [CrossRef]
3. Konsolakis, M.; Lykaki, M. Recent Advances on the Rational Design of Non-Precious Metal Oxide Catalysts Exemplified by CuO_x/CeO_2 Binary System: Implications of Size, Shape and Electronic Effects on Intrinsic Reactivity and Metal-Support Interactions. *Catalysts* **2020**, *10*, 160. [CrossRef]
4. Melchionna, M.; Fornasiero, P. The role of ceria-based nanostructured materials in energy applications. *Mater. Today* **2014**, *17*, 349–357. [CrossRef]
5. Tang, W.-X.; Gao, P.-X. Nanostructured cerium oxide: Preparation, characterization, and application in energy and environmental catalysis. *MRS Commun.* **2016**, *6*, 311–329. [CrossRef]
6. Cortés Corberán, V.; Rives, V.; Stathopoulos, V. Chapter 7—Recent Applications of Nanometal Oxide Catalysts in Oxidation Reactions. In *Advanced Nanomaterials for Catalysis and Energy*; Elsevier Inc.: Amsterdam, The Netherlands, 2019; pp. 227–293. [CrossRef]
7. Paier, J.; Penschke, C.; Sauer, J. Oxygen Defects and Surface Chemistry of Ceria: Quantum Chemical Studies Compared to Experiment. *Chem. Rev.* **2013**, *113*, 3949–3985. [CrossRef] [PubMed]
8. Zhang, D.; Du, X.; Shi, L.; Gao, R. Shape-controlled synthesis and catalytic application of ceria nanomaterials. *Dalton Trans.* **2012**, *41*, 14455–14475. [CrossRef] [PubMed]
9. Qiao, Z.-A.; Wu, Z.; Dai, S. Shape-Controlled Ceria-based Nanostructures for Catalysis Applications. *ChemSusChem* **2013**, *6*, 1821–1833. [CrossRef]
10. Sun, C.; Xue, D. Size-dependent oxygen storage ability of nano-sized ceria. *Phys. Chem. Chem. Phys.* **2013**, *15*, 14414–14419. [CrossRef]
11. Aneggi, E.; Wiater, D.; De Leitenburg, C.; Llorca, J.; Trovarelli, A. Shape-Dependent Activity of Ceria in Soot Combustion. *ACS Catal.* **2014**, *4*, 172–181. [CrossRef]
12. Li, L.; Han, W.; Tang, Z.; Zhang, J.; Lu, G. Hard-template synthesis of three-dimensional mesoporous Cu-Ce based catalysts with tunable architectures and their application in the CO catalytic oxidation. *RSC Adv.* **2016**, *6*, 64247–64257. [CrossRef]
13. Zhu, W.; Tang, K.; Li, J.; Liu, W.; Niu, X.; Zhao, G.; Ma, X.; Liu, Z.; Wei, H.; Yang, Y. The effect of copper species in copper-ceria catalysts: Structure evolution and enhanced performance in CO oxidation. *RSC Adv.* **2016**, *6*, 46966–46971. [CrossRef]
14. Gu, Z.; Li, K.; Qing, S.; Zhu, X.; Wei, Y.; Li, Y.; Wang, H. Enhanced reducibility and redox stability of Fe_2O_3 in the presence of CeO_2 nanoparticles. *RSC Adv.* **2014**, *4*, 47191–47199. [CrossRef]
15. Damaskinos, C.M.; Vasiliades, M.A.; Stathopoulos, V.N.; Efstathiou, A.M. The Effect of CeO_2 Preparation Method on the Carbon Pathways in the Dry Reforming of Methane on Ni/CeO_2 Studied by Transient Techniques. *Catalysts* **2019**, *9*, 621. [CrossRef]
16. Konsolakis, M. Recent Advances on Nitrous Oxide (N_2O) Decomposition over Non-Noble-Metal Oxide Catalysts: Catalytic Performance, Mechanistic Considerations, and Surface Chemistry Aspects. *ACS Catal.* **2015**, *5*, 6397–6421. [CrossRef]
17. Zou, W.; Ge, C.; Lu, M.; Wu, S.; Wang, Y.; Sun, J.; Pu, Y.; Tang, C.; Gao, F.; Dong, L. Engineering the NiO/CeO_2 interface to enhance the catalytic performance for CO oxidation. *RSC Adv.* **2015**, *5*, 98335–98343. [CrossRef]
18. Lykaki, M.; Pachatouridou, E.; Carabineiro, S.A.C.; Iliopoulou, E.; Andriopoulou, C.; Kallithrakas-Kontos, N.; Boghosian, S.; Konsolakis, M. Ceria nanoparticles shape effects on the structural defects and surface chemistry: Implications in CO oxidation by Cu/CeO_2 catalysts. *Appl. Catal. B Environ.* **2018**, *230*, 18–28. [CrossRef]
19. Lykaki, M.; Stefa, S.; Carabineiro, S.A.C.; Pandis, P.K.; Stathopoulos, V.N.; Konsolakis, M. Facet-Dependent Reactivity of Fe_2O_3/CeO_2 Nanocomposites: Effect of Ceria Morphology on CO Oxidation. *Catalysts* **2019**, *9*, 371. [CrossRef]
20. Konsolakis, M.; Lykaki, M.; Stefa, S.; Carabineiro, S.A.C.; Varvoutis, G.; Papista, E.; Marnellos, G.E. CO_2 Hydrogenation over Nanoceria-Supported Transition Metal Catalysts: Role of Ceria Morphology (Nanorods versus Nanocubes) and Active Phase Nature (Co versus Cu). *Nanomaterials* **2019**, *9*, 1739. [CrossRef]
21. Konsolakis, M.; Sgourakis, M.; Carabineiro, S.A.C. Surface and redox properties of cobalt-ceria binary oxides: On the effect of Co content and pretreatment conditions. *Appl. Surf. Sci.* **2015**, *341*, 48–54. [CrossRef]

22. Konsolakis, M.; Ioakimidis, Z.; Kraia, T.; Marnellos, G.E. Hydrogen Production by Ethanol Steam Reforming (ESR) over CeO_2 Supported Transition Metal (Fe, Co, Ni, Cu) Catalysts: Insight into the Structure-Activity Relationship. *Catalysts* **2016**, *6*, 39. [CrossRef]
23. Zhu, H.; Chen, Y.; Wang, Z.; Liu, W.; Wang, L. Catalytic oxidation of CO over mesoporous copper-doped ceria catalysts *via* a facile CTAB-assisted synthesis. *RSC Adv.* **2018**, *8*, 14888–14897. [CrossRef]
24. Qiu, N.; Zhang, J.; Wu, Z. Peculiar surface-interface properties of nanocrystalline ceria-cobalt oxides with enhanced oxygen storage capacity. *Phys. Chem. Chem. Phys.* **2014**, *16*, 22659–22664. [CrossRef] [PubMed]
25. Konsolakis, M.; Carabineiro, S.A.C.; Papista, E.; Marnellos, G.E.; Tavares, P.B.; Agostinho Moreira, J.; Romaguera-Barcelay, Y.; Figueiredo, J.L. Effect of preparation method on the solid state properties and the deN_2O performance of CuO-CeO_2 oxides. *Catal. Sci. Technol.* **2015**, *5*, 3714–3727. [CrossRef]
26. Wu, K.; Sun, L.-D.; Yan, C.-H. Ceria-Based Nanocatalysts: Recent Progress in Well-Controlled Synthesis of Ceria-Based Nanocatalysts towards Enhanced Catalytic Performance. *Adv. Energy Mater.* **2016**, *6*. [CrossRef]
27. Devaiah, D.; Thrimurthulu, G.; Smirniotis, P.G.; Reddy, B.M. Nanocrystalline alumina-supported ceria-praseodymia solid solutions: Structural characteristics and catalytic CO oxidation. *RSC Adv.* **2016**, *6*, 44826–44837. [CrossRef]
28. Chen, L.; Weng, D.; Si, Z.; Wu, X. Synergistic effect between ceria and tungsten oxide on WO_3–CeO_2–TiO_2 catalysts for NH_3-SCR reaction. *Prog. Nat. Sci. Mater. Int.* **2012**, *22*, 265–272. [CrossRef]
29. Chen, F.; Ho, P.; Ran, R.; Chen, W.; Si, Z.; Wu, X.; Weng, D.; Huang, Z.; Lee, C. Synergistic effect of CeO_2 modified TiO_2 photocatalyst on the enhancement of visible light photocatalytic performance. *J. Alloys Compd.* **2017**, *714*, 560–566. [CrossRef]
30. Lamallem, M.; El Ayadi, H.; Gennequin, C.; Cousin, R.; Siffert, S.; Aïssi, F.; Aboukaïs, A. Effect of the preparation method on Au/Ce-Ti-O catalysts activity for VOCs oxidation. *Catal. Today* **2008**, *137*, 367–372. [CrossRef]
31. Chang, K.; Wang, T.; Chen, J.G. Hydrogenation of CO_2 to methanol over $CuCeTiO_x$ catalysts. *Appl. Catal. B Environ.* **2017**, *206*, 704–711. [CrossRef]
32. Ding, J.; Zhong, Q.; Zhang, S. A New Insight into Catalytic Ozonation with Nanosized Ce–Ti Oxides for NO_x Removal: Confirmation of Ce–O–Ti for Active Sites. *Ind. Eng. Chem. Res.* **2015**, *54*, 2012–2022. [CrossRef]
33. Li, P.; Xin, Y.; Li, Q.; Wang, Z.; Zhang, Z.; Zheng, L. Ce-Ti Amorphous Oxides for Selective Catalytic Reduction of NO with NH_3: Confirmation of Ce-O-Ti Active Sites. *Environ. Sci. Technol.* **2012**, *46*, 9600–9605. [CrossRef] [PubMed]
34. Yang, X.; Kattel, S.; Senanayake, S.D.; Anibal Boscoboinik, J.; Nie, X.; Graciani, J.; Rodriguez, J.A.; Liu, P.; Stacchiola, D.J.; Chen, J.G. Low Pressure CO_2 Hydrogenation to Methanol over Gold Nanoparticles Activated on a CeO_x/TiO_2 Interface. *J. Am. Chem. Soc.* **2015**, *137*, 10104–10107. [CrossRef] [PubMed]
35. Deng, W.; Dai, Q.; Lao, Y.; Shi, B.; Wang, X. Low temperature catalytic combustion of 1,2-dichlorobenzene over CeO_2–TiO_2 mixed oxide catalysts. *Appl. Catal. B Environ.* **2016**, *181*, 848–861. [CrossRef]
36. Li, S.; Zhu, H.; Qin, Z.; Wang, G.; Zhang, Y.; Wu, Z.; Li, Z.; Chen, G.; Dong, W.; Wu, Z.; et al. Morphologic effects of nano CeO_2-TiO_2 on the performance of Au/CeO_2-TiO_2 catalysts in low-temperature CO oxidation. *Appl. Catal. B Environ.* **2014**, *144*, 498–506. [CrossRef]
37. Vieira, G.B.; José, H.J.; Peterson, M.; Baldissarelli, V.Z.; Alvarez, P.; De Fátima Peralta Muniz Moreira, R. CeO_2/TiO_2 nanostructures enhance adsorption and photocatalytic degradation of organic compounds in aqueous suspension. *J. Photochem. Photobiol. A Chem.* **2018**, *353*, 325–336. [CrossRef]
38. Qu, X.; Xie, D.; Gao, L.; Du, F. Synthesis and photocatalytic activity of TiO_2/CeO_2 core-shell nanotubes. *Mater. Sci. Semicond. Process.* **2014**, *26*, 657–662. [CrossRef]
39. Ameen, S.; Shaheer Akhtar, M.; Seo, H.-K.; Shin, H.-S. Solution-processed CeO_2/TiO_2 nanocomposite as potent visible light photocatalyst for the degradation of bromophenol dye. *Chem. Eng. J.* **2014**, *247*, 193–198. [CrossRef]
40. Chen, Y.-J.; Xiao, G.; Wang, T.-S.; Zhang, F.; Ma, Y.; Gao, P.; Zhu, C.-L.; Zhang, E.; Xu, Z.; Li, Q. Synthesis and enhanced gas sensing properties of crystalline CeO_2/TiO_2 core/shell nanorods. *Sens. Actuators B Chem.* **2011**, *156*, 867–874. [CrossRef]
41. Tian, J.; Sang, Y.; Zhao, Z.; Zhou, W.; Wang, D.; Kang, X.; Liu, H.; Wang, J.; Chen, S.; Cai, H.; et al. Enhanced Photocatalytic Performances of CeO_2/TiO_2 Nanobelt Heterostructures. *Small* **2013**, *9*, 3864–3872. [CrossRef]
42. Fan, Z.; Meng, F.; Gong, J.; Li, H.; Hu, Y.; Liu, D. Enhanced photocatalytic activity of hierarchical flower-like CeO_2/TiO_2 heterostructures. *Mater. Lett.* **2016**, *175*, 36–39. [CrossRef]

43. Wang, Y.; Zhao, J.; Wang, T.; Li, Y.; Li, X.; Yin, J.; Wang, C. CO_2 photoreduction with H_2O vapor on highly dispersed CeO_2/TiO_2 catalysts: Surface species and their reactivity. *J. Catal.* **2016**, *337*, 293–302. [CrossRef]
44. Samadi, S.; Asadi Cordshooli, G.; Yousefi, M.; Kalateh, K.; Zakaria, S. CeO_2/TiO_2 core/shell nanoparticles as quantitative gas sensor at room temperature. *Sens. Rev.* **2018**, *38*, 458–466. [CrossRef]
45. Miah, A.T.; Malakar, B.; Saikia, P. Gold over Ceria-Titania Mixed Oxides: Solar Light Induced Catalytic Activity for Nitrophenol Reduction. *Catal. Lett.* **2016**, *146*, 291–303. [CrossRef]
46. Gao, X.; Du, X.; Cui, L.; Fu, Y.; Luo, Z.; Cen, K. A Ce-Cu-Ti oxide catalyst for the selective catalytic reduction of NO with NH_3. *Catal. Commun.* **2010**, *12*, 255–258. [CrossRef]
47. Du, X.; Wang, X.; Chen, Y.; Gao, X.; Zhang, L. Supported metal sulfates on Ce–TiO_x as catalysts for NH_3–SCR of NO: High resistances to SO_2 and potassium. *J. Ind. Eng. Chem.* **2016**, *36*, 271–278. [CrossRef]
48. Shi, Z.; Yang, P.; Tao, F.; Zhou, R. New insight into the structure of CeO_2-TiO_2 mixed oxides and their excellent catalytic performances for 1,2-dichloroethane oxidation. *Chem. Eng. J.* **2016**, *295*, 99–108. [CrossRef]
49. Gao, X.; Jiang, Y.; Zhong, Y.; Luo, Z.; Cen, K. The activity and characterization of CeO_2-TiO_2 catalysts prepared by the sol-gel method for selective catalytic reduction of NO with NH_3. *J. Hazard. Mater.* **2010**, *174*, 734–739. [CrossRef]
50. Muñoz-Batista, M.J.; Fernández-García, M.; Kubacka, A. Promotion of CeO_2-TiO_2 photoactivity by g-C_3N_4: Ultraviolet and visible light elimination of toluene. *Appl. Catal. B Environ.* **2015**, *164*, 261–270. [CrossRef]
51. Yao, X.; Zhao, R.; Chen, L.; Du, J.; Tao, C.; Yang, F.; Dong, L. Selective catalytic reduction of NO_x by NH_3 over CeO_2 supported on TiO_2: Comparison of anatase, brookite, and rutile. *Appl. Catal. B Environ.* **2017**, *208*, 82–93. [CrossRef]
52. Fang, Q.; Liang, X. CeO_2–Al_2O_3, CeO_2–SiO_2, CeO_2–TiO_2 core-shell spheres: Formation mechanisms and UV absorption. *RSC Adv.* **2012**, *2*, 5370–5375. [CrossRef]
53. Gao, X.; Jiang, Y.; Fu, Y.; Zhong, Y.; Luo, Z.; Cen, K. Preparation and characterization of CeO_2/TiO_2 catalysts for selective catalytic reduction of NO with NH_3. *Catal. Commun.* **2010**, *11*, 465–469. [CrossRef]
54. Soler, L.; Casanovas, A.; Urrich, A.; Angurell, I.; Llorca, J. CO oxidation and COPrOx over preformed Au nanoparticles supported over nanoshaped CeO_2. *Appl. Catal. B Environ.* **2016**, *197*, 47–55. [CrossRef]
55. Piumetti, M.; Andana, T.; Bensaid, S.; Russo, N.; Fino, D.; Pirone, R. Study on the CO Oxidation over Ceria-Based Nanocatalysts. *Nanoscale Res. Lett.* **2016**, *11*, 165. [CrossRef] [PubMed]
56. Mock, S.A.; Sharp, S.E.; Stoner, T.R.; Radetic, M.J.; Zell, E.T.; Wang, R. CeO_2 nanorods-supported transition metal catalysts for CO oxidation. *J. Colloid Interface Sci.* **2016**, *466*, 261–267. [CrossRef] [PubMed]
57. Elias, J.S.; Risch, M.; Giordano, L.; Mansour, A.N.; Shao-Horn, Y. Structure, Bonding, and Catalytic Activity of Monodisperse, Transition-Metal-Substituted CeO_2 Nanoparticles. *J. Am. Chem. Soc.* **2014**, *136*, 17193–17200. [CrossRef] [PubMed]
58. Stöber, W.; Fink, A.; Bohn, E. Controlled growth of monodisperse silica spheres in the micron size range. *J. Colloid Interface Sci.* **1968**, *26*, 62–69. [CrossRef]
59. Du Fresne von Hohenesche, C.; Stathopoulos, V.; Unger, K.K.; Lind, A.; Lindén, M. Formation of hierarchically ordered silicas prepared by spray drying of nanosized spheres. *Stud. Surf. Sci. Catal.* **2002**, *144*, 339–346. [CrossRef]
60. Stathopoulos, V.N.; Belessi, V.C.; Costa, C.N.; Neophytides, S.; Falaras, P.; Efstathiou, A.M.; Pomonis, P.J. Catalytic activity of high surface area mesoporous Mn-based mixed oxides for the deep oxidation of methane and lean-NO_x reduction. *Stud. Surf. Sci. Catal.* **2000**, *130*, 1529–1534. [CrossRef]
61. Salmas, C.E.; Stathopoulos, V.N.; Pomonis, P.J.; Androutsopoulos, G.P. Pore Structure-Chemical Composition Interactions of New High Surface Area Manganese Based Mesoporous Materials. Materials Preparation, Characterization, and Catalytic Activity. *Langmuir* **2002**, *18*, 423–432. [CrossRef]
62. Xu, J.; Harmer, J.; Li, G.; Chapman, T.; Collier, P.; Longworth, S.; Tsang, S.C. Size dependent oxygen buffering capacity of ceria nanocrystals. *Chem. Commun.* **2010**, *46*, 1887–1889. [CrossRef] [PubMed]
63. Barthos, R.; Hegyessy, A.; Klébert, S.; Valyon, J. Vanadium dispersion and catalytic activity of Pd/VO_x/SBA-15 catalysts in the Wacker oxidation of ethylene. *Microporous Mesoporous Mater.* **2015**, *207*, 1–8. [CrossRef]
64. Li, P.; Chen, X.; Li, Y.; Schwank, J.W. A review on oxygen storage capacity of CeO_2-based materials: Influence factors, measurement techniques, and applications in reactions related to catalytic automotive emissions control. *Catal. Today* **2019**, *327*, 90–115. [CrossRef]
65. Sebastiammal, S.S.; Shally, V.; Priyadharshini, M.; Jayam, S.G. Structural and optical properties of Cerium oxide nanoparticles. *Int. J. Eng. Trends Technol.* **2017**, *49*, 69–73. [CrossRef]

66. Babitha, K.K.; Sreedevi, A.; Priyanka, K.P.; Sabu, B.; Varghese, T. Structural characterization and optical studies of CeO_2 nanoparticles synthesized by chemical precipitation. *Indian J. Pure Appl. Phys.* **2015**, *53*, 596–603.
67. Ali, M.M.; Mahdi, H.S.; Parveen, A.; Azam, A. Optical properties of cerium oxide (CeO_2) nanoparticles synthesized by hydroxide mediated method. *AIP Conf. Proc.* **2018**, *1953*, 030044. [CrossRef]
68. Zhao, H.; Dong, Y.; Jiang, P.; Wang, G.; Zhang, J. Highly Dispersed CeO_2 on TiO_2 Nanotube: A Synergistic Nanocomposite with Superior Peroxidase-Like Activity. *ACS Appl. Mater. Interfaces* **2015**, *7*, 6451–6461. [CrossRef]
69. Fang, J.; Bao, H.; He, B.; Wang, F.; Si, D.; Jiang, Z.; Pan, Z.; Wei, S.; Huang, W. Interfacial and Surface Structures of CeO_2−TiO_2 Mixed Oxides. *J. Phys. Chem. C* **2007**, *111*, 19078–19085. [CrossRef]
70. Abdullah, H.; Khan, M.R.; Pudukudy, M.; Yaakob, Z.; Ismail, N.A. CeO_2-TiO_2 as a visible light active catalyst for the photoreduction of CO_2 to methanol. *J. Rare Earths* **2015**, *33*, 1155–1161. [CrossRef]
71. Lu, X.; Li, X.; Qian, J.; Miao, N.; Yao, C.; Chen, Z. Synthesis and characterization of CeO_2/TiO_2 nanotube arrays and enhanced photocatalytic oxidative desulfurization performance. *J. Alloys Compd.* **2016**, *661*, 363–371. [CrossRef]
72. Ansari, A.A.; Labis, J.; Alam, M.; Ramay, S.M.; Ahmad, N.; Mahmood, A. Physicochemical and Redox Characteristics of Fe Ion-doped CeO_2 Nanoparticles. *J. Chin. Chem. Soc.* **2015**, *62*, 925–932. [CrossRef]
73. Bespalko, Y.; Kuznetsova, T.; Kriger, T.; Chesalov, Y.; Lapina, O.; Ishchenko, A.; Larina, T.; Sadykov, V.; Stathopoulos, V. $La_2Zr_2O_7$/$LaAlO_3$ composite prepared by mixing precipitated precursors: Evolution of its structure under sintering. *Mater. Chem. Phys.* **2020**, *251*, 123093. [CrossRef]
74. Castanet, U.; Feral-Martin, C.; Demourgues, A.; Neale, R.L.; Sayle, D.C.; Caddeo, F.; Flitcroft, J.M.; Caygill, R.; Pointon, B.J.; Molinari, M.; et al. Controlling the {111}/{110} Surface Ratio of Cuboidal Ceria Nanoparticles. *ACS Appl. Mater. Interfaces* **2019**, *11*, 11384–11390. [CrossRef] [PubMed]
75. Wang, J.; Li, Z.; Zhang, S.; Yan, S.; Cao, B.; Wang, Z.; Fu, Y. Enhanced NH_3 gas-sensing performance of silica modified CeO_2 nanostructure based sensors. *Sens. Actuators B Chem.* **2018**, *255*, 862–870. [CrossRef]
76. Phokha, S.; Pinitsoontorn, S.; Maensiri, S. Structure and Magnetic Properties of Monodisperse Fe^{3+}-doped CeO_2 Nanospheres. *Nano-Micro Lett.* **2013**, *5*, 223–233. [CrossRef]
77. Mukherjee, D.; Rao, B.G.; Reddy, B.M. CO and soot oxidation activity of doped ceria: Influence of dopants. *Appl. Catal. B Environ.* **2016**, *197*, 105–115. [CrossRef]
78. Wu, Z.; Li, M.; Overbury, S.H. On the structure dependence of CO oxidation over CeO_2 nanocrystals with well-defined surface planes. *J. Catal.* **2012**, *285*, 61–73. [CrossRef]
79. Johnston-Peck, A.C.; Senanayake, S.D.; Plata, J.J.; Kundu, S.; Xu, W.; Barrio, L.; Graciani, J.; Sanz, J.F.; Navarro, R.M.; Fierro, J.L.G.; et al. Nature of the Mixed-Oxide Interface in Ceria-Titania Catalysts: Clusters, Chains, and Nanoparticles. *J. Phys. Chem. C* **2013**, *117*, 14463–14471. [CrossRef]